



HAL
open science

Computations of refractory linings structures under thermal loadings

Philippe Boisse, Alain Gasser, Jérôme Rousseau

► **To cite this version:**

Philippe Boisse, Alain Gasser, Jérôme Rousseau. Computations of refractory linings structures under thermal loadings. *Advances in Engineering Software*, 2002, 33 (7-10), pp.487-496. 10.1016/S0965-9978(02)00064-9 . hal-00021127

HAL Id: hal-00021127

<https://hal.science/hal-00021127>

Submitted on 18 Mar 2018

HAL is a multi-disciplinary open access archive for the deposit and dissemination of scientific research documents, whether they are published or not. The documents may come from teaching and research institutions in France or abroad, or from public or private research centers.

L'archive ouverte pluridisciplinaire **HAL**, est destinée au dépôt et à la diffusion de documents scientifiques de niveau recherche, publiés ou non, émanant des établissements d'enseignement et de recherche français ou étrangers, des laboratoires publics ou privés.

Computations of refractory lining structures under thermal loadings

P. Boisse*, A. Gasser, J. Rousseau

LMSP, UMR CNRS-ENSAM-ESEM, ESEM, 8, rue Léonard de Vinci, 45072 Orleans, France

Refractory linings are used to protect the exterior metallic part of some vessels containing very hot fluids. They are submitted to high thermomechanical loading that can lead to cracking. A local approach is first presented in order to analyse the refractory lining as a 3D domain. A smeared crack model is used to compute the damage in the refractory. Comparison with experiments on a refractory wall containing metal parts is performed in order to validate the 3D numerical computations. Some type of refactorised vessels (e.g. some steel ladles) can directly be analysed from this 3D modelling. Since some other refactorised vessel contains a very large number of metallic parts (such as tubes or anchors), it cannot be possible to compute such a global structure with this 3D analysis. Consequently, an approach has been developed based on a two-layer shell equivalent to the lining including the metallic casing with tubes and the refractory. The thermal and mechanical parameters of the model are identified with an inverse method, using results of 3D calculations performed with the local model defined previously. An experimental validation is made by a bending test, performed on a large refractory lining specimen. In the case of a cyclone of coal-fired power plant, the equivalent shell permits to compute the damage of the refractory in the global structure.

Keywords: Equivalent composite shell; Inverse method; Smeared crack model; Thermomechanical structural analysis; Refractory linings

1. Introduction

Structures containing very hot fluids such as steel ladles [1–3] or coal-fired power plants [4,5] comprise refractory linings that protect the steel structure (casing). These linings can be anchored or not on the exterior metallic envelope. The aim of this study is the numerical prediction of the refractory lining behaviour under thermomechanical loading. For example, in a coal-fired plant, the refractory castable is anchored to the steel support structure. Because of temperature gradient and thermal expansion which are different in castable and metal, high level stress occurs within the castable, during heating or cooling stages, that often leads to damage of the refractory and sometime to failure [6–8].

Three different scales can be differentiated in this problem. The first is the local scale at the vicinity of metallic parts such as tubes or anchors, the second the scale of a wall of the vessel made of the metallic envelope and the refractory. It can include metallic elements such as tubes and anchors (meso-scale). The third scale is that of the

global structure (macro-scale). To compute a structure like a metallurgic reactor or a coal-fired plant, it can or cannot be possible to use a 3D finite element model to analyse the refractory mechanical behaviour depending on the design of the structure. In some cases there are too many details (such as tubes or anchors). The solution proposed for this last case in this paper consists in identifying the thermal and mechanical behaviour parameters of an equivalent two-layer composite shell element in order to reduce the size of the computation model while accounting the effect of metallic local details such as tubes and computing the damage of the refractory (Fig. 1). An orthotropic material is considered for the cold layer, which models metallic casing tubes and a small part of the refractory. The second layer models the castable (that can be anchored). The behaviour of this layer has to model the damageable behaviour of the castable. The parameters of this shell element are obtained from an inverse approach using information given by some 3D calculations performed at the local scale. A bending test on a large specimen shows the agreement of the computations made with the two-layer shell element with the experimental results. The damage of a complete coal-fired plant cyclone under thermal loading is done with the equivalent shell approach. Because the calculated damage is

* Corresponding author. Fax: +33-1-44-24-64-68.
E-mail address: philippe.boisse@paris.ensam.fr (P. Boisse).

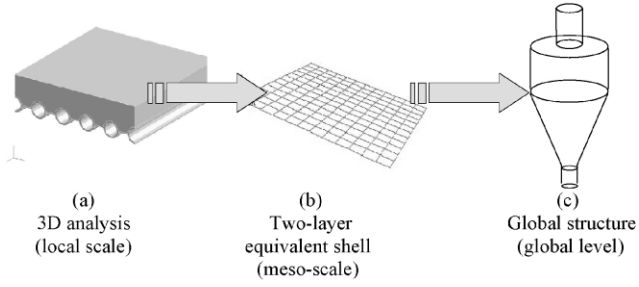


Fig. 1. Principle of structure computing using a simplified element accounting for the 3D mechanical behaviour.

larger than the real one, it is then investigated to account for expansion joints in the equivalent shell definition.

2. Analysis of the lining mechanical behaviour at local scale

2.1. Modelling

A 3D structural analysis is performed in the vicinity of a metallic part embedded in a castable (or juxtaposed). This analysis is made at the scale of a typical mechanical part such as tubes or anchors (some centimetres large), i.e. at the local scale (a) of Fig. 1. An elastic–plastic mechanical behaviour is considered for the steel (Table 1). The behaviour of the refractory castable (made with silicon carbide) is like the behaviour of concrete, i.e. very different in tension and compression (Fig. 2):

- elastic–plastic in compression;
- elastic–damageable in tension (an unloading goes back to zero), with softening after the elastic part [9,10].

It is modelled using a smeared crack model. The cracks are taken into account as a loss of stiffness and not as macro-cracks: the displacement u_{ck} due to the crack opening is transformed in strain ε_{ck} with a characteristic length h :

$$\varepsilon_{ck} = \frac{u_{ck}}{h} \quad (1)$$

Several types of smeared crack models are existing [11]:

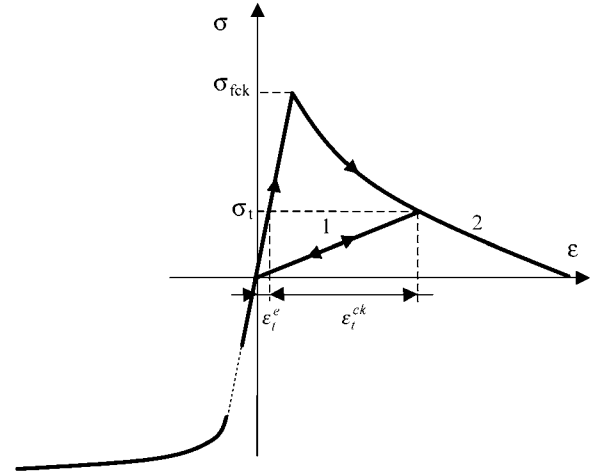


Fig. 2. Uniaxial behaviour with tension softening and plasticity in compression (the dotted line in compression shows that the stresses reached in compression are very higher than in tension).

- with one fixed crack [12]: one crack appears perpendicular to the maximum principal tensile stress (in mode I) and then stays fixed during further loading;
- with one rotating crack [13,14]: one crack appears perpendicular to the maximum principal stress and then rotates to stay perpendicular to this maximum principal tensile stress for further loading;
- with multiple fixed cracks [15,16]: it is the same as that of the one fixed crack model but other cracks can appear (for further loading) perpendicular to the first one.

Here, it is the multiple fixed crack model which is used [17]: the crack directions are fixed, but it is possible to have three orthogonal cracks in 3D.

A significant advantage of this type of model is that the computation algorithms are in a close form of those classically used for plasticity, such as prediction–correction methods [18–20]. When the material is under tension, cracking is assumed to occur when the stresses reach a failure surface, which is called ‘crack detection surface’. This crack detection surface (represented in 2D in Fig. 3) is given by Eq. (2)

$$f = q - \left(3 - b \frac{\sigma_t}{\sigma_{fck}}\right)p - \left(2 - \frac{b}{3} \frac{\sigma_t}{\sigma_{fck}}\right)\sigma_t = 0 \quad (2)$$

Table 1
Mechanical and thermal properties of steel and refractory

Property	Steel	Refractory	
Thermal conductivity, λ ($\text{W m}^{-1} \text{°C}^{-1}$)	52	1.2 at 500 °C	5.5 at 1000 °C
Specific heat, C_p ($\text{J kg}^{-1} \text{°C}^{-1}$)	469	1000	
Young’s modulus, E (GPa)	208	65	
Poisson’s ratio, ν	0.3	0.16	
Thermal expansion, α (°C^{-1})	11.4×10^{-6}	5×10^{-6}	
Elasticity limit stress (MPa) (first cracking stress for the refractory)	335	15.2	
Softening slope, a (MPa)	–	–11	

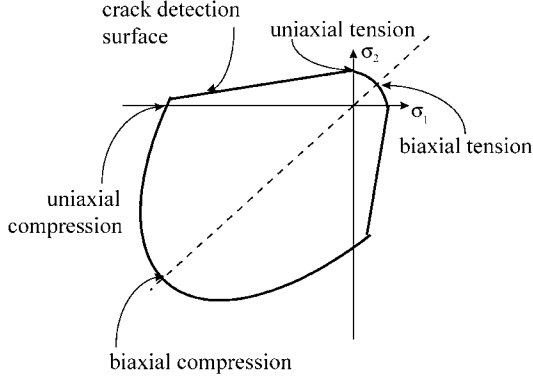


Fig. 3. Crack detection surface in tension, and plastic yield surface in compression (in the plane σ_2 versus σ_1).

with

$$p = -\frac{1}{3}\text{trace}(\sigma), \quad q = \sqrt{\frac{3}{2}\mathbf{S} : \mathbf{S}}, \quad \mathbf{S} = \sigma + p\mathbf{I} \quad (3)$$

where σ_{fck} is the stress of first cracking in uniaxial tension (Fig. 2), p the effective pressure stress, q the Von Mises equivalent deviatoric stress, b a constant, and σ_t is the equivalent uniaxial tensile stress. A strain rate decomposition into elastic and inelastic strain rates is used

$$d\epsilon_t = d\epsilon_t^e + d\epsilon_t^{ck} \quad (4)$$

where $d\epsilon_t$ is the total strain rate, $d\epsilon_t^e$ is the elastic strain rate, and $d\epsilon_t^{ck}$ is the inelastic strain rate associated with the crack detection surface.

The flow rule is given by:

$$d\epsilon_t^{ck} = d\lambda \frac{\partial f}{\partial \sigma} \quad \text{If } f = 0 \text{ and } d\lambda > 0 \quad (5)$$

or else

$$d\epsilon_t^{ck} = 0$$

Once the first crack appears, its direction is stored, and the damage elasticity is used to model the failed material. The elasticity is written in the form

$$\sigma = \mathbf{D} : \epsilon^e \quad (6)$$

where \mathbf{D} is the elastic stiffness matrix for the castable. The determination of \mathbf{D} is described below.

Let n a cracked direction, with corresponding stress α_{nn} and elastic strain ϵ_{nn}^e . Let ϵ_{nn}^{\max} be the maximum value of ϵ_{nn}^e during the all history of the loading, and σ_{nn}^{\max} the corresponding stress. If ϵ_{nn}^e is positive (i.e. tension), there are two cases to determine D_{nnnn} : if $\epsilon_{nn}^e < \epsilon_{nn}^{\max}$, then (part 1 of the curve, Fig. 2)

$$D_{nnnn} = \frac{\sigma_{nn}^{\max}}{\epsilon_{nn}^{\max}} \quad (7)$$

if $\epsilon_{nn}^e = \epsilon_{nn}^{\max}$, then (part 2 of the curve, Fig. 2)

$$D_{nnnn} = \frac{\partial \sigma_{nn}}{\partial \epsilon_{nn}} \quad (8)$$

The model accounts for the anisotropy created by the cracking. The crack direction is fixed during all the computation but one or two complementary crack directions can appear during the loading. The model neglects permanent strains associated to cracks, i.e. it is possible that cracks can close when the stress becomes negative.

2.2. Parameters identification

For simplification, the softening part is modelled as a straight line of slope a . As a result, the tension behaviour is characterised by three parameters: the Young modulus E , the stress of first cracking σ_{fck} , and the softening slope a . Since it is not easy to perform accurate tension tests on castable specimens, these parameters are identified using a four-point bending test [21] which gives a curve load F versus displacement u . Since a bending test (specially when the mechanical behaviour is non-linear) is a structural test with tension and compression, a direct identification is not possible: an inverse method is necessary.

The bending test is simulated with the finite element method using an initial set of parameters.

A residual vector \mathbf{r} (difference between the experimental measures F^{ex} and the finite element values F^{fe} for given displacements u_s) is defined as:

$$r_i = F_i^{\text{fe}}(u_s) - F_i^{\text{ex}}(u_s) \quad (9)$$

An error function e (least square error) is then calculated

$$e(\mathbf{m}) = \frac{1}{2} \sum_{i=1}^n [r_i(\mathbf{m})]^2 \quad (10)$$

where $\mathbf{m}(E, \sigma_{fck}, a)$ is the set of p parameters ($p = 3$) to be identified, and n the number of experimental values (n must be greater than p ; here $n = 10$).

The error function must take into account some constraints C_j on the parameters (E and σ_{fck} , positive, a negative). If they are q constraints (here $q = 3$), the error becomes

$$e^*(\mathbf{m}) = e(\mathbf{m}) + \sum_{j=1}^q \frac{\omega_j}{C_j(\mathbf{m})} \quad (11)$$

with $C_j(\mathbf{m}) \geq 0$, $j = 1, \dots, q$

where ω_j is the weight of constraint j . The minimisation of this error function (i.e. the optimisation of the parameters) is made by the Levenberg–Marquardt method [22,23]. At iteration k , an increment of the parameters $d\mathbf{m}^{(k)}$ is calculated by

$$[(\mathbf{J}^{(k)})^T (\mathbf{J}^{(k)}) + \lambda^{(k)} \mathbf{I} + \mathbf{H}^{(k)}] d\mathbf{m}^{(k)} = -(\mathbf{J}^{(k)})^T \mathbf{r}^{(k)} + \mathbf{f}^{(k)} \quad (12)$$

where $\lambda^{(k)}$ is the positive Levenberg–Marquardt parameter at iteration k , \mathbf{J} is the jacobian matrix of e^* , \mathbf{f} and \mathbf{H} are the first and the second derivatives of penalty functions ξ ,

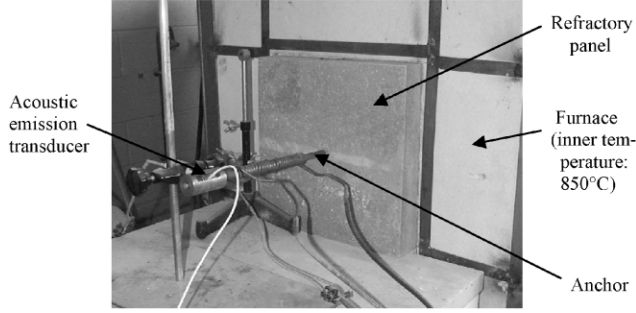


Fig. 4. Thermal cycling experimental device with acoustic measurement.

respectively, in regard to the parameters:

$$J_{i\alpha} = \frac{\partial F_i^{\text{fe}}}{\partial m_\alpha}, \quad \xi_j = \frac{\omega_j}{C_j(\mathbf{m})}, \quad f_\alpha = - \sum_{j=1}^q \frac{\partial \xi_j}{\partial m_\alpha}, \quad (13)$$

$$H_{\alpha\beta} = \sum_{j=1}^q \frac{\partial^2 \xi_j}{\partial m_\alpha \partial m_\beta}$$

The finite element results for the set of parameters \mathbf{m} and for p parameters, where the value of m_α is perturbed, gives the jacobian matrix \mathbf{J} :

$$J_{i\alpha} = \frac{F_i^{\text{fe}}(m_1, m_2, \dots, m_\alpha + dm_\alpha, \dots, m_p) - F_i^{\text{fe}}(m_1, m_2, \dots, m_\alpha, \dots, m_p)}{dm_\alpha} \quad (14)$$

This method gives after several iterations the values of the three parameters (Table 1).

2.3. 3D simulations

To validate the mechanical behaviour modelling presented above, some experimental thermomechanical tests have been performed on panels ($300 \times 300 \times 80 \text{ mm}^3$) with one or two metallic anchors [24,25]. A special furnace (Fig. 4) was built to reproduce the thermomechanical conditions of the refractory linings in coal-fired plants (850 °C on the



Fig. 5. Pull-out test.

inner-face, 350 °C on the back-face, with thermal cyclic loading).

The measure of the acoustic emission allows us to follow the crack opening around the anchor (these cracks are mostly radial for axisymmetric anchors), to obtain the temperature of first cracking, and to observe that the first thermal cycle is the most damaging for the refractory (until 200,000 acoustic events at the end of firing [26]). This experiment is interesting because it gives information on cracking and it is non-destructive. Nevertheless, it is also important to measure quantitative values of damage. Therefore, mechanical tests are necessary. Pull-out tests (Fig. 5) are used here. After the panel has submitted the thermal loading of the special furnace, it is fixed on a tensile device, and the anchor is pulled out, at room temperature, using the wave guide (linked to the anchor). The load versus displacement curve allows us to quantify the loss of stiffness (linked to the level of damage). One can also observe that the failure surface is a cone (Fig. 5).

These two tests described above are then analysed with a finite element approach using the material model given in Section 2.2. The panels contain an axisymmetric anchor (\emptyset 16 mm, length: 48 mm). They could be modelled in 3D (one quarter of a panel, Fig. 6), or in 2D (axisymmetric, Fig. 7). The results are almost identical. The simulation of the firing of the panel (Fig. 6, inner face at 850 °C, back face at 350 °C) shows that the cracks are mostly radial (like the experimental results), and gives a temperature of first cracking near the one obtained by acoustic emission. The simulation of the pull-out test (Fig. 7, top face fixed, anchor pulled out downwards) shows that the failure is a cone, and that the loss of stiffness is in good agreement with the experimental load versus displacement curve. Therefore, these tests and simulations allow us to validate the material model of the castable.

These 3D analyses can be used for the structural computation of some applications, such as steel ladles [27] because the geometry of the metallic parts is not so complicated. So, the approach presented above can be used for a global computation. A steel ladle allows to carry liquid steel at 1650 °C. It is made up of several layers:

- a metallic structure,
- a thin insulation layer,
- a safety layer made with castable,
- a wear layer, made with refractory bricks, in contact with the liquid steel.

The 3D finite element model (representing one quarter of the ladle, Fig. 8(a)) has 50,000 degrees of freedom and is based on 20-nodes hexahedral elements. The loading is as follows:

- prescribed cyclic temperature for the inner face (wear layer), corresponding to the filling and emptying of the ladle;

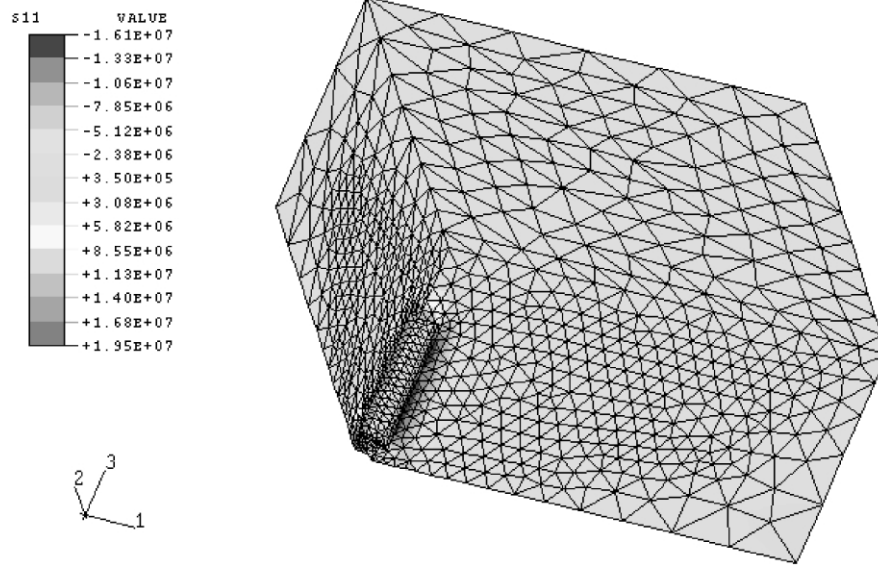


Fig. 6. Stresses 11 in one quarter of a panel with an axisymmetric anchor (after firing: inner face at 850 °C and back face at 350 °C).

- convection and radiation for the exterior face (metallic structure);
- gravity.

The simulation of the ladle submitted to this loading, and hold by its trunnions, leads in a realistic computational time (10 h on a HP-PA8200 processor) to significant results on displacements and stresses in the refractorised structure at different stages of the thermomechanical loading cycle. For example, Fig. 8 shows the plastic strains in the metallic structure and the damaged zones in the safety layer after 10 cycles (full ladle). This model brings a help during the design of the ladle to minimise the damage in the refractory linings.

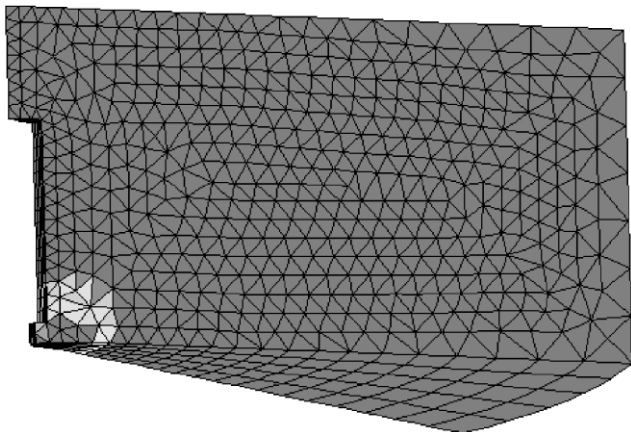


Fig. 7. Damage in the castable around the anchor after a pull-out test (axisymmetric analysis, top face fixed, anchor pulled out downwards).

3. Analysis of the lining mechanical behaviour using a equivalent two-layer shell element

3.1. Shell analyses versus 3D computations

When the geometry of the lining is complex, i.e. when it is composed of many components such as metallic tubes (Fig. 1(a)) or anchors [25,28], the 3D analysis described above (and that is directly used in some cases of steel ladles) is not more possible. The solution proposed in this section, in order to analyse the global structure in a reasonable computing time while calculating the damage of the refractory, consists in defining an equivalent shell element (Fig. 9). This shell is composed of two layers:

- the first one is made with an elastic–orthotropic behaviour (casing with tubes in one direction), with 9 coefficients (mechanical coefficients E_{1a} , E_{2a} , ν_{12a} , G_{12a} , G_{13a} , G_{23a} , thermal expansion α_a , conductivity λ_a , specific heat C_{pa});
- the second one with an elastic–damageable behaviour (refractory lining), with 7 coefficients: E_b , ν_b , stress of first cracking σ_{fck} , slope of softening a (which is assumed to be constant for simplicity reasons), α_b , λ_b , C_{pb} .

To identify the shell mechanical and thermal parameters, tension, bending, shear and thermal experimental tests should be necessary. But, it is very difficult to perform this complete set of experimental tests (determining the 16 parameters) on real panels of refractory linings. To avoid this practical difficulty, 3D analyses are performed on a model based on the analysis at the local scale previously presented. A representative cell (with several tubes, Fig. 9(a)) is computed both with the 3D model and with

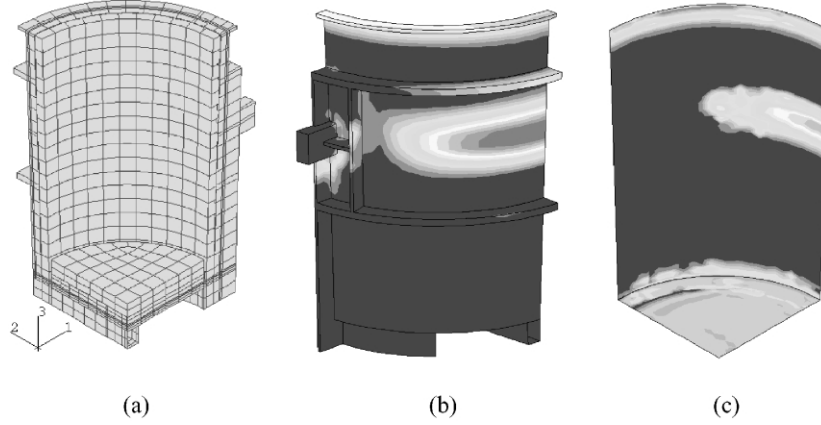


Fig. 8. Steel ladle: (a) mesh, (b) plastified zones in the metallic structure, (c) damaged zones in the safety layer.

the shell elements. Comparison between both these models (for all tests) allows with an inverse scheme to identify the shell behaviour parameters.

3.2. Determination of the shell coefficients

To identify the shell coefficients, the inverse method presented in Section 2.2 was used, with 16 parameters ($p = 16$). Several tests (simulated in 3D) are necessary:

- two tension tests (in two different directions, Fig. 10(a)),
- two four-point bending tests (in two different directions, Fig. 10(b)),
- an in-plane shear test (Fig. 10(c)),
- a transient thermal test (the temperature is prescribed on a face) [29],
- a thermal test on a panel submitted to an uniform temperature (to obtain the thermal expansion) [29].

From these 3D tests, some quantities (like reaction forces, displacements, or temperatures), noted F_i^{3D} , are chosen for given values of loading (displacement or temperature), noted ε_i . These quantities are the values that we would like to find again with the shell model. Therefore, the tests described above are simulated using the two layer shell elements. The obtained quantities (for the given values of loading ε_i) are noted F_i^S , and compared to F_i^{3D} , with the

residual vector \mathbf{r}

$$r_i = F_i^S(\varepsilon_i) - F_i^{3D}(\varepsilon_i) \quad (15)$$

that allows to define the corresponding least square error e given by Eq. (10). The minimisation of this error by the Levenberg–Marquardt method gives the optimised parameters.

To simplify this identification, it was taken into account that some parameters are independent. So, the method was divided in three steps. The first is the identification of the 8 elastic parameters (E_{1a} , E_{2a} , ν_{12a} , G_{12a} , G_{13a} , G_{23a} , E_b , ν_b) using the two tension tests, the two four-point bending tests and the in-plane shear test (Fig. 10). The second step is the identification of the two damage parameters (σ_{fck} , a) of the damageable layer, using the two tension tests (in the tube direction and in the perpendicular direction, Fig. 10(a)). Fig. 11 gives the results obtained in both 3D and shell analyses with the identified damage parameters. And finally, the third step allows to determine the six thermomechanical parameters (λ_a , C_{pa} , α_a , λ_b , C_{pb} , α_b) using the two thermal tests described above [30].

The 16 parameters obtained are given in Table 2. To validate them numerically, two tests (which were not used for the identification) were simulated. The first is a panel under pressure with fixed edges. The comparison of the displacements obtained independently by both 3D and shell models (Fig. 12) shows that the differences are smaller than 8%. This validates the elastic parameters

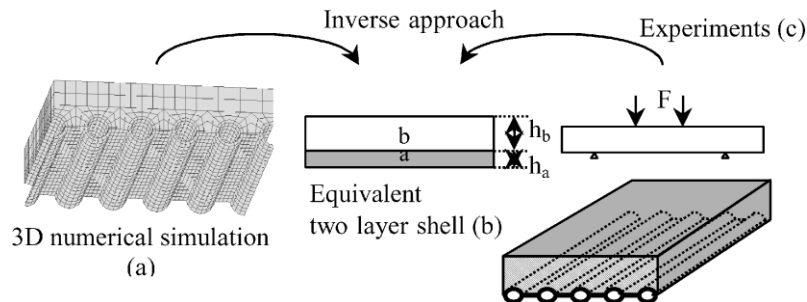


Fig. 9. Equivalent two-layer shell element obtained from 3D computations at the level of the anchor and experiments.

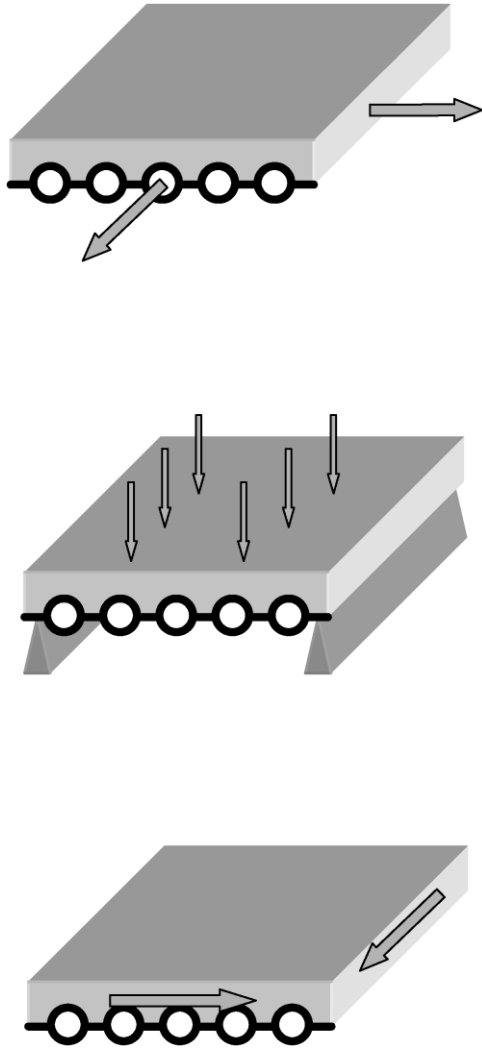


Fig. 10. 3D analyses for the shell elastic coefficient calculation. (a) Tensions; calculation of E_b , ν_b , E_{1a} , E_{2a} , ν_{12a} . (b) Four-point bending; calculation of G_{13b} , G_{23b} . (c) In-plane shear; calculation of G_{12a} .

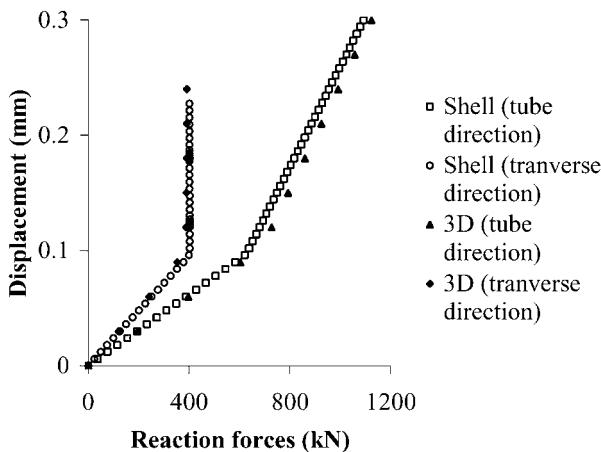


Fig. 11. Displacement–reaction forces curves in tension, in both directions, taking into account damage.

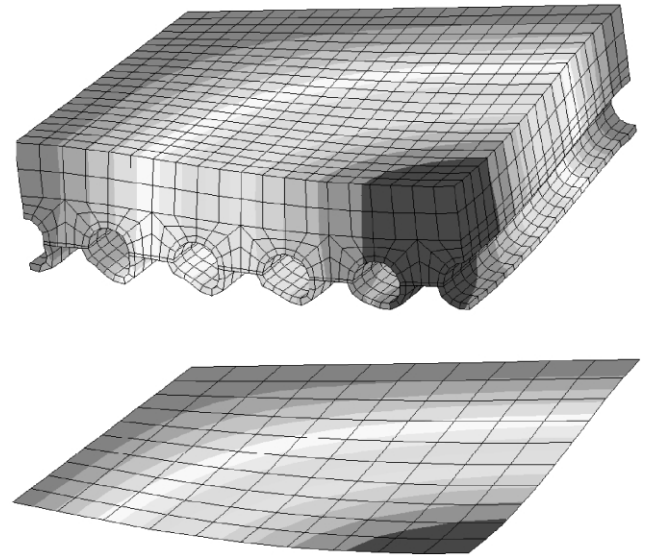


Fig. 12. Validation case: panel under constant pressure and clamped edges. Comparison between displacements for 3D and shell analyses (one quarter of the structure).

In order to validate the damage parameters, the shear test presented in Fig. 10(c) is performed independently by both 3D and shell models (this shear damage test has not been used for the identification of the damage parameters). The comparison of the results is presented in Fig. 13. They present a good agreement.

3.3. Experimental validation

To validate the presented shell approach, an experimental verification was performed using four-point bending tests on refractory lining specimens (1.2 m long) with several tubes and anchors. The simulation (on one half of the panel, Fig. 14) shows a good agreement with the experiments for the load/displacement curve (Fig. 15) and the damaged zones at the top of the tubes.

3.4. Structural analysis of a tubed cyclone

As an application of this two layer shell element, the computation of a tubed cyclone (part of a coal-fired power

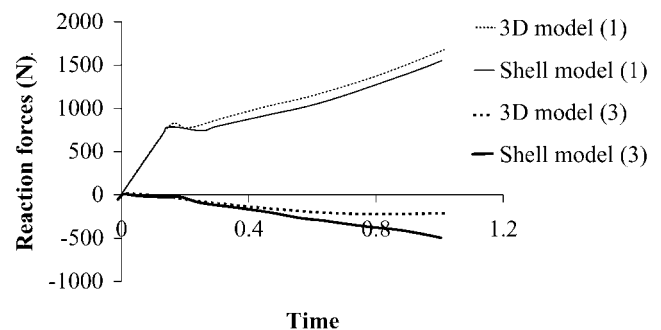


Fig. 13. Comparison of reaction forces in shear (shell and 3D models) in directions 1 and 3.

Table 2
Identified parameters of the two layer shell element

	Material A (orthotropic)	Material B (isotropic damageable)
Elastic properties	$E_{1a} = 5.05 \times 10^4$ MPa $E_{2a} = 1.81$ MPa $\nu_{12a} = 0.303$ $G_{12a} = 9.09 \times 10^3$ MPa $G_{13a} = 454$ MPa $G_{23a} = 18.2$ MPa	$E_b = 4.93 \times 10^4$ MPa $\nu_b = 0.175$
Damage parameters	–	$\sigma_{fck} = 13$ MPa $a = -8.13 \times 10^{-3}$ MPa
Thermal conductivity (W/m °C)	$\lambda_a = 0.463$	$\lambda_b = 1.86$ (at 200 °C), 4.47 (at 500 °C)
Specific heat (J/kg °C)	$C_a = 51$	$C_b = 894$
Thermal expansion (°C ⁻¹)	$\alpha_a = 6.69 \times 10^{-6}$	$\alpha_b = 4.43 \times 10^{-6}$

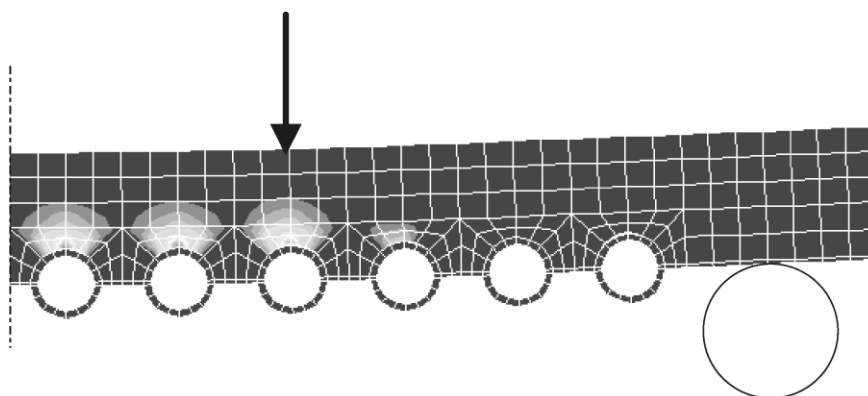


Fig. 14. Finite element analysis of the four-point bending test: displacement of the half of the refractory lining specimen, and damaged zones (at the top of the tubes).

plant, 10 m high) under thermal loading is presented. The temperature is prescribed on the inner face (850 °C) and on the outer face (350 °C). The gravity is taken into account. The cyclone is fixed at its top.

The damaged zones are presented in Fig. 16. They are very large, more that observed in the existing structure. Indeed, the shell element does not take into account the expansion joints, which are present in this type of vessel between the panels of refractory linings. These joints play an important role in the level of stresses. Consequently, it is

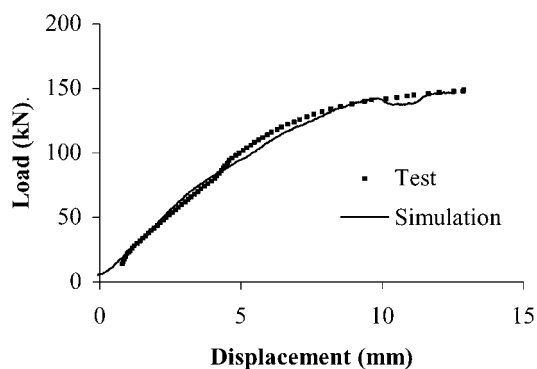


Fig. 15. Comparison of the experimental and numerical load/displacement curves for a four-point bending test on a refractory lining specimen.

necessary to account for them in the equivalent shell element when the calculated structure involves such joints.

4. Expansion joints

To take into account the expansion joints, the above approach is used within a simplified finite element. Different numerical tests on an elementary cell containing two perpendicular joints (Fig. 17) are performed. A compression test on this 3D cell shows a uniaxial behaviour with two slopes (Fig. 18): the change of slope corresponds to the joint closure. Therefore, the two-layer shell element will have twice more coefficients according to whether the joints are open or closed. This work is in progress and results on complete structural analyses will be presented in a next paper.

5. Conclusions

The thermomechanical analyses of refractory linings can be based on local calculations using a smeared crack model. When the geometry of the vessel walls is complex, it has

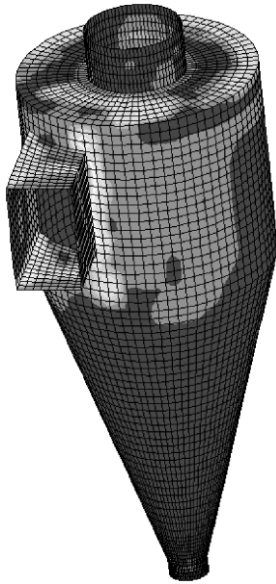


Fig. 16. Damaged zones in a cyclone of coal-fired power plant (internal face).

been shown that equivalent shell elements can be used. The thermal and mechanical properties of a two-layer composite shell have been optimised using 3D computations at the local scale and inverse methods. It has been verified experimentally that this equivalent shell approach describes fairly well the mechanical and thermal responses of the global refractorised vessels. It brings help for the design of structures with refractory linings. The damaged zones can be located. It is then possible to decrease their size in changing the castable composition, the type of anchors or the shape of the structure. It is also possible, using a submodelling and the analysis at the local scale, to obtain more precise information on cracking in important damaged parts. Nevertheless, to obtain good results on a complete structure, it is necessary to account for the expansion joints in the equivalent shell formulation. Some studies are currently in progress on this point.

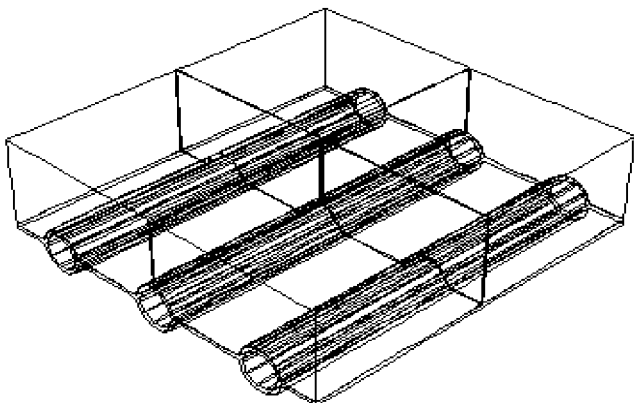


Fig. 17. Representative elementary cell ($500 \times 500 \text{ mm}^2$) with two perpendicular joints.

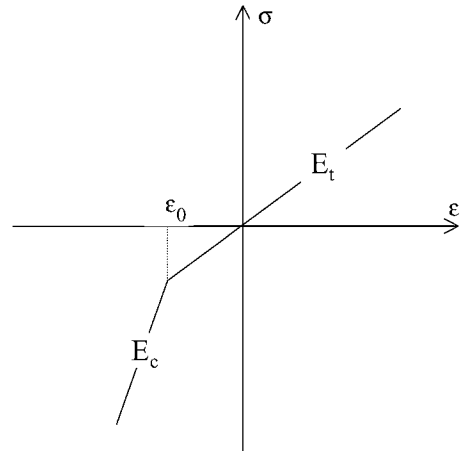


Fig. 18. Tension/compression behaviour of a representative elementary cell with two perpendicular joints.

Acknowledgements

The authors acknowledge the support provided by Electricité de France and Sollac/Usinor companies. They also acknowledge Y. Dutheillet (EDF) and J. Poirier (Sollac/Usinor) for their collaboration.

References

- [1] Gaston A, Medina M. Thermal modelling of casting ladles: high alumina, dolomite, magnesite and magnesia-graphite refractories. *Iron Steelmaker* 1996;29–35.
- [2] Poirier J. Recent tendencies in refractories in relation with service in the steel industry. *Proceedings of 39th Colloquium on Refractories*, Aachen, Germany; 1996. p. 6–16.
- [3] Peruzzi S, Poirier J, Glandus JC, Huger M. Numerical study of the in-service behaviour of refractory parts used in continuous casting. *Proceedings of Sixth ECERS Conference*, Brighton, UK; 1999. p. 161–2.
- [4] Gordon ED. Refractories in CFB applications. *Proceedings of the 12th International Conference On Fluidized Bed Combustions*, San Diego, California; 1993.
- [5] Andrieux C, Boisse P, Dutheillet Y, Gabis V, Gasser A, Rousseau J. Modelling and design of an anchored refractory lining. *Proceedings of UNITECR'99*, Berlin, Germany; 1999. p. 10–2.
- [6] Bergmann B, Wagner H, Bannenberg N. Lining life of steel ladles in secondary metallurgy. *La Revue Métallurgie CIT* 1989;311–6.
- [7] Russell RO, Hallum GW, Chen ES. Thermomechanical studies of obround ladles during preheating and use. *Iron Steelmaker* 1993; 37–43.
- [8] Vert T, Fitzpatrick G, Stacey J. Steelmaking ladle refractories at Dofasco. *ISS Steelmaking Conference Proceedings*; 1995. p. 547–50.
- [9] Hillerborg A, Modeer M, Petersson PE. Analysis of crack formation and growth in concrete by means of fracture mechanics and finite elements. *Cement Concrete Res* 1976;6:773–82.
- [10] Cotterell B, Mai YW. *Fracture mechanics of cementitious materials*. Glasgow: Blackie; 1996.
- [11] Weihe S, Kröplin B, de Borst R. Classification of smeared crack models based on materials and structural properties. *Int J Solids Struct* 1998;35(12):1289–308.
- [12] Rashid YR. Ultimate strength analysis of prestressed concrete pressure vessels. *Nucl Engng Des* 1968;7(4):334–44.
- [13] Cope RJ, Rao PV, Clark LA, Norris P. Modelling of reinforced

- concrete behaviour for finite element analyses of bridge slabs. Numerical methods for nonlinear problems I, New York: Taylor & Francis; 1980. p. 457–70.
- [14] Bazant ZP. Comment on orthotropic models for concrete and geomaterials. *J Engng Mech ASCE* 1983;109(3):849–65.
- [15] De Borst R, Nauta P. Non-orthogonal cracks in a smeared finite element model. *Engng Comput* 1985;2:35–46.
- [16] Hibbitt, Karlsson, Sorensen. Theoretical manual of Abaqus code, version 5.7, HKS Inc.; 1997.
- [17] Gasser A, Boisse P, Dutheillet Y, Poirier J. Experimental and numerical analyses of thermomechanical refractory lining behaviour. *J Mater: Des Appl (IMechE, Part L)* 2001;245:41–54.
- [18] Simo JC, Taylor R. Consistent tangent operators for rate independent elastoplasticity. *Comput Meth Appl Mech Engng* 1984;48:101–18.
- [19] Simo JC, Taylor R. A return mapping algorithm for plane stress elastoplasticity. *Int J Numer Meth Engng* 1986;22:649–70.
- [20] Crisfield MA. Non-linear finite element analysis of solids and structures. Advanced topics, 2. New York: Wiley; 1997. p. 135–57.
- [21] Lemaistre H. Etude des propriétés thermomécaniques de divers réfractaires. PhD Thesis. INSA Lyon, France; 1998.
- [22] Marquardt DW. An algorithm for least squares estimation of nonlinear parameters. *J Soc Ind Appl Math* 1963;11(2):431–41.
- [23] Schnur DS, Zabarás N. An inverse method for determining elastic material properties and a material interface. *Int J Numer Meth Engng* 1992;33:2039–57.
- [24] Andrieux C, Gabis V, Gasser A, Boisse P, Rezakhanlou R. Castable anchoring optimisation to improve service life of refractory linings. Proceedings of UNITECR'97; 1997. p. 317–26.
- [25] Mamdy-Andrieux C. Analyse et simulation des contraintes d'origine thermique sur des structures réfractaires de centrales LFC. PhD Thesis. University of Orléans, France; 1999.
- [26] Andrieux C, Boisse P, Dutheillet Y, Gabis V, Gasser A, Rousseau J. Two layer composite shell for anchored refractory lining computing. Proceedings of ICCM12, Paris, France; 1999.
- [27] Derré V, Gasser A, Boisse P. Poche à acier de 270 tonnes à tenue améliorée. Report for Usinor; 2000.
- [28] Tassot P, Poirier J, Masse F. Model investigations and improvement of injection lance for hot metal pretreatment steel refining. Proceedings of UNITECR'89, Anaheim, USA; 1989. p. 109–20.
- [29] Boisse P, Gasser A, Poirier J, Rousseau J. Simulations of thermomechanical behaviour of composite refractory linings. *Composites, Part B* 2001;32(5):461–74.
- [30] Rousseau J, Gasser A, Boisse P. Formulation d'un matériau équivalent pour la simulation du comportement d'un élément de paroi de cyclone de centrale LFC. Report for EDF; 1999.